Time-dependent Monte Carlo simulations of critical and Lifshitz points of the axial-next-nearest-neighbor Ising model

Roberto da Silva[*]
Instituto de Fisica, Universidade Federal do Rio Grande do Sul, Avenida Bento Gonçalves 9500, CEP 91501-970, Porto Alegre, Rio Grande do Sul, Brazil

Nelson Alves, Jr.[†] and Jose Roberto Drugowich de Felício[‡]
Faculdade de Filosofia, Ciências e Letras de Ribeirão Preto, Universidade de São Paulo, Avenida Bandeirantes, 3900, CEP 14040-901, Ribeirão Preto, São Paulo, Brazil

(Received 23 October 2012; published 23 January 2013)

In this work, we study the critical behavior of second-order points, specifically the Lifshitz point (LP) of a three-dimensional Ising model with axial competing interactions [the axial-next-nearest-neighbor Ising (ANNNI) model], using time-dependent Monte Carlo simulations. We use a recently developed technique that helps us localize the critical temperature corresponding to the best power law for magnetization decay over time: $\langle M\rangle_{m_0=1} \sim t^{-\beta/\nu z}$, which is expected of simulations starting from initially ordered states. We obtain original results for the dynamic critical exponent z, evaluated from the behavior of the ratio $F_2(t) = \langle M^2\rangle_{m_0=0}/\langle M\rangle^2_{m_0=1} \sim t^{3/z}$, along the critical line up to the LP. We explore all the critical exponents of the LP in detail, including the dynamic critical exponent θ that characterizes the initial slip of magnetization and the global persistence exponent θ_g associated with the probability $P(t)$ that magnetization keeps its signal up to time t. Our estimates for the dynamic critical exponents at the Lifshitz point are $z = 2.34(2)$ and $\theta_g = 0.336(4)$, values that are very different from those of the three-dimensional Ising model (the ANNNI model without the next-nearest-neighbor interactions at the z axis, i.e., $J_2 = 0$), i.e., $z \approx 2.07$ and $\theta_g \approx 0.38$. We also present estimates for the static critical exponents β and ν, obtained from extended time-dependent scaling relations. Our results for static exponents are in good agreement with previous works.

DOI: 10.1103/PhysRevE.87.012131 PACS number(s): 05.70.Ln, 05.10.Ln, 02.70.Uu

I. INTRODUCTION

A. Modulated systems and the Lifshitz point

In condensed matter physics there are several models presenting spatial modulated structures of some local property such as the position of the particles, the magnetization, and the charge density [1]. Such modulation can be commensurate or incommensurate in relation to the underlying lattice. A phase is called commensurate if the ratio between the period of the modulation and the period of the lattice is a rational number. Otherwise, the phase is called incommensurate. The basic mechanism leading to modulation is the competition between interactions favoring distinct orderings [2]. For example, the modulated structures observed in rare-earth metals [3] were interpreted as a consequence of the competition generated by the spatially oscillatory Ruderman-Kittel-Yasuya-Yosida interaction [4–6]. In order to explain the spatial modulation found in erbium, Elliott introduced an Ising model [7], later named the axial-next-nearest-neighbor Ising (ANNNI) model [8]. It is one of the simplest models able to exhibit a rich phase diagram containing a complex region of spatially modulated phases [9–11]. The model is defined by the Hamiltonian

$$\mathcal{H} = -\sum_{x,y,z}[J_0(\sigma_{x+1,y,z} + \sigma_{x,y+1,z}) + J_1\sigma_{x,y,z+1} + J_2\sigma_{x,y,z+2}]\sigma_{x,y,z}, \quad (1)$$

where $\sigma_{x,y,z} = \pm 1$ is an Ising spin variable at the site (x,y,z) of a simple cubic lattice, J_0 is the nearest-neighbor interaction in the xy plane, and $J_1$and J_2 are the nearest- and next-nearest-neighbor interactions in the z direction.Here J_1 and J_2 compete and may have opposite or the same sign. However, when J_1 and J_2 have opposite signs, the competition between them may give rise to the modulated phases.

The mean-field phase diagram of the model displaying the main commensurate phases in the plane of the reduced temperature kT/J_1 against the competition parameter $-J_2/J_1$, shown in Fig. 1, was obtained by Bak and von Boehm [12] and is divided into three major regions: the modulated region M and the paramagnetic P and ferromagnetic F phases. In this diagram, as well as throughout the paper, we set $J_0 = J_1$. The paramagnetic phase is separated from the ferromagnetic phase and the modulated region by critical lines P-F and P-M, respectively. In contrast, a first-order transition F-M takes place between the ferromagnetic phase and the modulated region. The critical line P-M belongs to the universality class of the XY model, whereas the critical line P-F presents an Ising-like critical behavior [13]. The transition lines P-F, P-M, and F-M meet at the Lifshitz point (LP), introduced theoretically by Hornreich *et al.* [14]. The location of the LP in the phase diagram of the ANNNI model was obtained initially from a high-temperature series technique [15]. However, the precise location of the LP is difficult to obtain because, close to it, one meets the challenging task of dealing with modulated phases of very large periods. Thus, subsequent attempts to locate the LP were made. Single spin-flip Monte Carlo simulations were performed along the P-F critical line

[*]rdasilva@if.ufgrs.br
[†]nalves@if.usp.br
[‡]drugo@usp.br

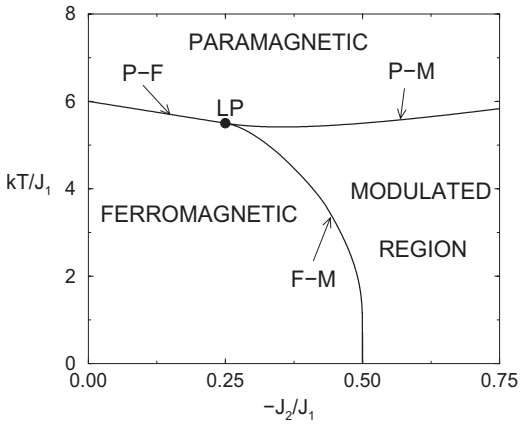

FIG. 1. Mean-field phase diagram of the ANNNI model, displaying the ferromagnetic phase, the paramagnetic phase, and the modulated region. The critical lines P-F and P-M meet the first-order phase transition line F-M at the Lifshitz point (LP) (see the text).

towards the LP [16,17], thus avoiding the modulated region. Despite the successful results obtained from these works, it was only recently that the Lifshitz point was located with high precision [18] by means of a new variation of the cluster Wolf algorithm [19]. Concerning the critical properties of the LP, it was shown that this multicritical point belongs to neither the universality class of the XY model nor the one of the Ising model [14]. This fact gave rise to much interest in the study of the particular critical behavior of a LP. Thus the critical properties of the LP found in the phase diagram of the ANNNI model were widely studied by several approaches [20,21], including ϵ expansions [14], a high-temperature series technique [21], and Monte Carlo (MC) simulations [17]. Experimentally, the most complete results concerning the LP were obtained for the magnetic compound MnP, which exhibits a LP belonging to the universality class of the LP present in the ANNNI model [22–24]. Here it is important to mention that although this model has been widely explored by methods from equilibrium statistical mechanics, there are no results for the three-dimensional (3D) ANNNI model obtained by an approach that deals with MC simulations performed far from equilibrium [25] that will be employed in this paper. However, we remark that several works in the literature have previously used a dynamical approach to study the Lifshitz points. For example, the critical dynamics of relaxation of the model near the Lifshitz point has been studied by the ε expansion and the exponent z was numerically estimated for uniaxial and biaxial cases [26]. Alternatively, in Ref. [27] the growth of an order parameter is studied when a system at Lifshitz point is quenched from the homogeneous disordered state to the ordered state where correlation and structure factors after quench in this system are analyzed via renormalization-group method. Numerical estimates of exponent z are supplied in this same reference. Studies about the dynamics of the ANNNI model were developed, though in two-dimensional versions of the model, but such works do not explore critical properties. For example, in Refs. [28,29] the kinetics of domain growth of the one- and two-dimensional anisotropic ANNNI models was explored via Monte Carlo methods using Glauber and heat-bath multispin dynamics, respectively. In the following section we briefly present the nonequilibrium approach to be used in our analysis.

B. Nonequilibrium critical dynamics

The study of critical properties originated from statistical fluctuations of spin systems became possible in the nonequilibrium stage after the seminal ideas of Janssen, Schaub, and Schmittmann [30] and Huse [31]. By quenching systems from high temperatures to the critical one, they have shown that universality and scaling behavior appear even in the early stages of time evolution via renormalization-group techniques and numerical calculations, respectively. Hence, by using short-time dynamics, one can often circumvent the well-known problem of the critical slowing down that plagues investigations of the long-time regime.

Here we briefly review finite-size scaling in the dynamics relaxation of spin systems. We present our alternative derivation of some power laws in the short-time dynamics context. Readers,who want a more complete review of this topic may want to read Refs. [32,33].

This topic is based on time-dependent simulations and constitutes an important issue in the context of phase transitions and critical phenomena. Such methods can be applied not only to estimate the critical parameters in spin systems, but also to calculate the critical exponents (static and dynamic ones) through different scaling relations by setting different initial conditions.

The dynamic scaling relation obtained by Janssen *et al.* for the kth moment of the magnetization is written as

$$\langle M^k\rangle(t,\tau,L,m_0) = b^{-k\beta/\nu}\langle M^k\rangle(b^{-z}t,b^{1/\nu}\tau,b^{-1}L,b^{x_0}m_0), \quad (2)$$

where the arguments are the time t; the reduced temperature $\tau = (T - T_c)/T_c$, with T_c being the critical one, the lattice linear size L; and the initial magnetization m_0. Here the operator $\langle\cdots\rangle$ denotes an average over different configurations due to different possible time evolutions from each initial configuration compatible with a given m_0.

On the right-hand side of Eq. (3) is an arbitrary spatial rescaling factor b and an anomalous dimension x_0 related to m_0. The exponents β and ν are the equilibrium critical exponents associated with the order parameter and the correlation length, respectively. The exponent z is the dynamic one, which characterizes the time correlations in equilibrium. After choosing $b^{-1}L = 1$, $T = T_c(\tau = 0)$, and $k = 1$ we obtain $\langle M\rangle(t,L,m_0) = L^{-\beta/\nu}\langle M\rangle(L^{-z}t,L^{x_0}m_0)$.

Setting $u = tL^{-z}$ and $w = L^{x_0}m_0$, we have $\langle M\rangle(u,w) = \langle M\rangle(L^{-z}t,L^{x_0}m_0)$. The derivative with respect to L is

$$\frac{\partial\langle M\rangle}{\partial L} = (-\beta/\nu)L^{-\beta/\nu-1}\langle M\rangle(u,w) + L^{-\beta/\nu}\left[\frac{\partial\langle M\rangle}{\partial u}\frac{\partial u}{\partial L} + \frac{\partial\langle M\rangle}{\partial w}\frac{\partial w}{\partial L}\right],$$

where we have explicitly $\partial u/\partial L = -ztL^{-z-1}$ and $\partial w/\partial L = x_0m_0L^{x_0-1}$. In the limit $L\to\infty$, $\partial_L\langle M\rangle\to 0$, we have $x_0w\frac{\partial\langle M\rangle}{\partial w} - zu\frac{\partial\langle M\rangle}{\partial u} - \beta/\nu\langle M\rangle = 0$. The separability of the variables u and w in $\langle M\rangle(u,w) = M_1(u)M_2(w)$ leads to $x_0wM_2'/M_2 = \beta/\nu + zuM_1'/M_2$, where the prime means the derivative with respect to the argument. Since the left-hand

side of this equation depends only on w and the right-hand side depends only on u, they must be equal to a constant c. Thus $M_1(u) = u^{(c/z)-\beta/(\nu z)}$ and $M_2(w) = w^{c/x_0}$, resulting in $\langle M\rangle(u,w) = m_0^{c/x_0} L^{\beta/\nu} t^{(c-\beta/\nu)/z}$. Returning to the original variables, we have $\langle M\rangle(t,L,m_0) = m_0^{c/x_0} t^{(c-\beta/\nu)/z}$.

On the one hand, choosing $c = x_0$ and calculating $\theta = (x_0 - \beta/\nu)/z$, at criticality ($\tau = 0$) we obtain

$$\langle M\rangle_{m_0} \sim m_0 t^{\theta}, \tag{3}$$

corresponding to a regime under small initial magnetization. This can be observed by a finite-time scaling $b = t^{1/z}$ in Eq. (2), at critical temperature $\tau = 0$, which leads to $\langle M\rangle(t,m_0) = t^{-\beta/(\nu z)}\langle M\rangle(1,t^{x_0/z}m_0)$. Defining $x = t^{x_0/z}m_0$, an expansion of the averaged magnetization around $x = 0$ results in $\langle M\rangle(1,x) = \langle M\rangle(1,0) + \partial_x\langle M\rangle|_{x=0}\, x + O(x^2)$. By construction $\langle M\rangle(1,0) = 0$, since $x = t^{x_0/z}m_0 \ll 1$ and $\partial_x\langle M\rangle|_{x=0}$ is a constant, discarding the quadratic terms we obtain the expected power-law behavior $\langle M\rangle_{m_0} \sim m_0 t^{\theta}$. This anomalous behavior of initial magnetization is valid only for a characteristic time scale $t_{\max} \sim m_0^{-z/x_0}$.

On the other hand, the choice $c = 0$ corresponds to the case in which the system does not depend on the initial trace and $m_0 = 1$ leads to a simple power law

$$\langle M\rangle_{m_0=1} \sim t^{-\beta/\nu z}, \tag{4}$$

which similarly corresponds to decay of magnetization for $t > t_{\max}$. The evaluation of critical exponents θ and $\beta/\nu z$ via Monte Carlo simulations concerns taking averages over different runs. In the second case, simpler simulations are considered because the system starts from the ferromagnetic (ordered) initial state. However, the first one is somewhat difficult to deal with since it demands working with prepared initial states with a precise value of m_0 (sharp preparation) besides the delicate limit $m_0 \to 0$.

An alternative way to determine this exponent was proposed in Ref. [34], where it was shown that the time correlation function of the order parameter also follows a power-law scale form at the short-time regime, i.e.,

$$Q(t) = \langle M(0)M(t)\rangle \sim t^{\theta}. \tag{5}$$

The main advantage in the use of Eq. (5) is that one does not need to fix precisely the initial order parameter m_0. The only requirement is that $\langle m_0\rangle = 0$, where $\langle(\cdots)\rangle$ stands for the average of the quantity $(\cdots)$ over different initial configurations. Now let us look at the second moment of magnetization. Since the spin-spin correlation $\langle\sigma_i\sigma_j\rangle$ is negligible for $m_0 = 0$, we have that for a fixed t,

$$\langle M^2\rangle_{m_0=0} = \frac{1}{L^{2d}}\sum_{i=1}^{L^d}\langle\sigma_i^2\rangle + \frac{1}{L^{2d}}\sum_{i}^{L^d}\langle\sigma_i\sigma_j\rangle \approx L^{-d}$$

and by considering the scaling relation (with $b = t^{1/z}$) for the second moment of magnetization, we have, according to Eq. (2),

$$\begin{aligned}\langle M^2\rangle_{m_0=0}(t,L) &\approx t^{-2\beta/\nu z}\langle M^2\rangle_{m_0=0}(1,bL)\\ &= t^{-2\beta/\nu z}(bL)^{-d} \sim t^{(d-2\beta/\nu)/z},\end{aligned} \tag{6}$$

where d is the system dimension.

Using Monte Carlo simulations, many authors have obtained the dynamic exponents θ and z, the static ones β and ν, and other specific exponents for several models: the Baxter-Wu model [35], the two-, three-, and four-state Potts models [36,37], the Ising model with multispin interactions [38], the Ising model with competing interactions [39], models with no defined Hamiltonian (cellular automata) [40], models with a tricritical point [41], the Heisenberg model [42], protein folding [43], and so on. The sequence to determine the static exponents from short-time dynamics is as follow: We first determine z, then perform Monte Carlo simulations that mix initial conditions [36], and finally consider the power law for the cumulant

$$F_2(t) = \frac{\langle M^2\rangle_{m_0=0}}{\langle M\rangle^2_{m_0=1}} \sim t^{d/z}. \tag{7}$$

This ratio has proven to be useful for the calculation of the exponent z for several spin models governed by Boltzmann-Gibbs statistical mechanics, but its application also includes models with spin flip based on generalized statistics [44]. In this technique, graphs of $\ln F_2$ against $\ln t$ lay on the same straight line for different lattice sizes, without any rescaling in time, yielding more precise estimates for z. Although it seems clear from Eq. (7), it is worth stressing here that two independent runs are necessary in order to calculate the ratio F_2: In one of them $m_0 = 0$, while in the other one $m_0 = 1$.

Equations (5), (3), and (7) solve the problem in determining the dynamic critical exponents θ and z. However, the ability of short-time Monte Carlo simulations goes beyond the evaluation of dynamic critical exponents in the sense that this technique also allows us to obtain the static critical exponents, which will be discussed in the following.

Starting from $m_0 = 1$, we have the expected power law described by Eq. (4); thus considering $\ln M(t,\tau)$, we must expect

$$\left.\frac{\partial \ln M(t,\tau)}{\partial\tau}\right|_{\tau=0} \sim t^{1/\nu z}, \tag{8}$$

which is obtained by differentiating the quantity $\ln M(t,\tau)$ in relation to reduced temperature $\tau = (T - T_c)/T_c$. When dealing with Monte Carlo simulations, the partial derivative is approximated in first order by the difference

$$\left.\frac{\partial \ln M(t,\tau)}{\partial\tau}\right|_{\tau=0} \approx \frac{1}{2\varepsilon}\ln\left[\frac{M(t,T_c+\varepsilon)}{M(t,T_c-\varepsilon)}\right], \tag{9}$$

where $\varepsilon \ll 1$. It is clear from Eq. (9) that two independent simulations are necessary to obtain the exponent $1/\nu z$: One of them evolves at temperature $T_c + \varepsilon$, whereas the other one evolves at $T_c - \varepsilon$.

Therefore, with $\widehat{z}$ estimated from Eq. (7) we obtain the estimated $\widehat{\nu}$ according to $\widehat{(\nu z)^{-1}}$, obtained from Eq. (8), by calculating the product

$$\widehat{\nu} = [\widehat{z}\cdot\widehat{(\nu z)^{-1}}]^{-1},$$

where the uncertainty in $\widehat{\nu}$ is calculated through uncertainty of z (σ_z) and the uncertainty of $\widehat{(\nu z)^{-1}}$ ($\sigma_{(\nu z)^{-1}}$), previously obtained by statistics over n_s different seeds, is calculated

according to the error propagation equation

$$\sigma_\nu = \sqrt{\frac{\sigma_z^2}{\widehat{z}^4\widehat{(\nu z)^{-1}}^2} + \frac{\sigma^2_{(\nu z)^{-1}}}{\widehat{z}^2\widehat{(\nu z)^{-1}}^4}}.$$

Finally, in order to obtain an estimate $\widehat{\beta}$, we first estimate $\widehat{\beta/\nu z}$ obtained from the magnetization decay (4) and after we perform the product

$$\widehat{\beta} = \widehat{(\beta/\nu z)} \cdot [\widehat{(\nu z)^{-1}}]^{-1}$$

and the propagated error is directly calculated as a function of the respective uncertainties

$$\sigma_\beta = \sqrt{\frac{\sigma^2_{(\beta/\nu z)}}{\widehat{(\nu z)^{-1}}^2} + \frac{\widehat{(\beta/\nu z)}^2\sigma^2_{(\nu z)^{-1}}}{\widehat{(\nu z)^{-1}}^4}}.$$

Here it is important to mention that the ratio β/ν should have been previously calculated by the evaluated $\widehat{\beta/\nu z}$ from Eq. (4) and $\widehat{z}$ from Eq. (7) such that

$$\widehat{\beta/\nu} = \widehat{(\beta/\nu z)} \cdot \widehat{z}. \tag{10}$$

Not only can quantities related to the moments of the magnetization explain the nonequilibrium aspects of phase transitions and critical phenomena, but also those related to the first-passage-time probabilities and variations of this topic (see, e.g., Refs. [45,46]). By considering this approach, under the same nonequilibrium conditions, a new exponent was initially proposed by Ref. [45]: the global persistence exponent θ_g. It is related to the probability $P(t)$ that the global order parameter has not changed sign up to time t after a quench to T_c, according to expected power-law behavior

$$P(t) \sim t^{-\theta_g}. \tag{11}$$

As argued by Majumdar *et al.* [45], if the dynamics of the global order parameter is described by a Markovian process, θ_g is not a new independent exponent and it can be related to other critical exponents

$$\theta_g z = \omega z - d + 1 - \eta/2, \tag{12}$$

where ω is the autocorrelation exponent in the expected power law [47] $A(t,t'=0)_{m_0=0} = (1/L^d)\langle\sum_i \sigma_i(t)\sigma_i(0)\rangle \sim t^{-\omega}$, where $\sigma_i(t)$ is the value of the spin variable s_i at the site i of a d-dimensional system of linear size L, assuming, at instant t, that z is the dynamic critical exponent defined as $\tau \sim \xi^z$, where τ and ξ are time and spatial correlation lengths, respectively. However, the time evolution of the order parameter is in general a non-Markovian process and θ_g turns out to be a new independent critical exponent describing the evolving of the stochastic dynamic process toward equilibrium.

In order to evaluate the persistence probability $P(t)$, we first define $\rho(t)$ as the fraction of runs for which the magnetization changes its sign for the first time at the instant t. Our probability $P(t)$ is numerically calculated from the cumulative distribution function of such $\rho(t)$. Thus $P(t)$ describes the probability that magnetization does not cross the origin up to time t,

$$P(t) = 1 - \sum_{t'=1}^{t} \rho(t'). \tag{13}$$

We start our simulations with a random initial condition, where $\langle m_0\rangle = 0$. Here it is important to mention that such a concept is very versatile and it has been applied to characterize several applications such as tricritical points [48], besides interdisciplinary applications such as the analysis of bankruptcies of players in public goods games [49] and econophysics [50]. Thus it can also be interesting to study, for example, Lifshitz points in spin models.

The goal of this paper is to expand our knowledge of the ANNNI model by studying the ferromagnetic-paramagnetic phase transition with particular attention given to the Lifshitz point. The layout of this paper is as follows. In Sec. II we give more details about numerical simulations that will be performed at the Lifshitz point. Moreover, we describe a simple method recently developed by da Silva *et al.* in Ref. [44] that refines the critical parameters based on the best determination coefficient in the linear fit $\ln\langle M\rangle$ versus $\ln t$. In this same section we present the first part of our results, where we explicitly show the refinement of critical temperatures of the second-order (ferromagnetic-paramagnetic) line up to the Lifshitz point. In Sec. III we present our estimates for the critical exponents and in this case we separate our results into two branches. In Sec. III A we evaluate critical exponents (only z and β/ν) for each temperature estimated along the critical line previously estimated by the refinement process. In these first calculations, the aim is only the monitoring of the behavior of these two exponents (one dynamic and the other static) to show the pronounced difference between Ising-like points and the Lifshitz point. In Sec. III B we present the complete results and studies for both dynamic (θ, θ_g, and z) and static (β and ν) critical exponents, specifically for the Lifshitz point, comparing the latter with results obtained in previous experimental and theoretical works. Finally, in Sec. IV we summarize and briefly discuss the main results of this paper.

II. MONTE CARLO SIMULATIONS

Monte Carlo simulations were performed on simple rectangular lattices with linear dimensions L_x, L_y, and L_z and periodic boundary conditions. The spin states were updated by using the one-spin-flip heat-bath algorithm, which was used as the basis for the result obtained by Henkel and Pleimling [18] for the location of the LP: ($-J_2/J_1 = 0.270 \pm 0.004$; $k_BT/J_1 = 3.7475 \pm 0.005$).

For the ANNNI model the order parameter corresponds to time-dependent magnetization, defined as an average over all $L_x \times L_y \times L_z$ spins and over the different N_s runs:

$$\langle M\rangle(t) = \frac{1}{n_s L^3}\sum_{i=1}^{n_s}\sum_{x,y,z}\sigma^{(i)}_{x,y,z}(t), \tag{14}$$

where the index $i = 1,\ldots,N_s$ denotes the corresponding run of a simulation. The ordered state is ferromagnetic, with all (or most of) the spins pointing either up or down. As discussed in the preceding section, the lattice's initial condition depends on the scaling relation considered: $\langle m_0\rangle = 0$ [Eq. (5)], $m_0 = 0$ [numerator of Eq. (7)], $m_0 = 1$ [Eqs. (4) and (9)], and m_0 fixed, but with random configurations considering a sharp preparation [Eq. (3)].

Here we address time-dependent MC simulations in the context of the so-called short-time dynamics. Before evaluation of some critical exponents and the complete study of the Lifshitz point (Sec. III), in this section we apply the refinement method to estimate the critical parameters of several points along the second-order line including the Lifshitz point itself.

The algorithm to estimate the critical temperature is divided into two stages: (i) a coarse-grained location and (ii) fine-scale refinement. In stage (i), since the magnetization must behave as a power law $\langle M\rangle \sim t^{-\beta/\nu z}$, by fixing a specific α value we conjecture that changing J_1/k_BT_c from $J_1/k_BT_c^{(\max)}$ up to $J_1/k_BT_c^{(\min)}$, the corresponding best $J_1/k_BT_c^{(\text{best})}$ is the one that leads to the best linear behavior of $\ln\langle M\rangle$ versus $\ln t$. We have considered $n_s = 400$ realizations, with initial magnetization $m_0 = 1$. For each $\alpha = -J_2/J_1$ changing from 0 up to 0.27, with displacement $\Delta\alpha = 0.03$ between the values, where $J_0 = J_1$ for all of our calculations, we changed J_1/k_BT_c from $J_1/k_BT_c^{(\max)} = 0.266\,844\,56\ldots$ up to $J_1/k_BT_c^{(\min)} = 0.221\,654\,13\ldots$. These extreme values were extracted from the literature since they correspond to the best-known estimates for the 3D Ising model ($\alpha = 0$, which corresponds to $k_BT_c/J = 4.511\,533\,335\,1\ldots$) and the LP ($\alpha = 0.27$, which corresponds to $k_BT_c/J = 3.7475\ldots$), respectively. Just as a safeguard, we enlarge this interval by performing $J_1/k_BT_c^{(\max,0)} = 0.28$ and $J_1/k_BT_c^{(\min,0)} = 0.21$.

Thus, for each input α value, by using $\Delta^{(0)}(J_1/k_BT_c) = 0.002$, we span our temperatures over a range described by parametrization $J_1/k_BT_c = J_1/k_BT_c^{(\min)} + j\Delta^{(0)}(J_1/k_BT_c)$, $j = 0,\ldots,32$, so for each temperature, a linear fit is performed and we calculate the determination coefficient of the fit as

$$r = \frac{\sum_{t=1}^{N_{\text{MC}}}(\overline{\ln\langle M\rangle} - a - b\ln t)^2}{\sum_{t=1}^{N_{\text{MC}}}[\overline{\ln\langle M\rangle} - \ln\langle M\rangle(t)]^2}, \tag{15}$$

with $\overline{\ln\langle M\rangle} = (1/N_{\text{MC}})\sum_{t=1}^{N_{\text{MC}}}\ln\langle M\rangle(t)$, where N_{MC} is the number of Monte Carlo sweeps. In our experiments we have used $N_{\text{MC}} = 150$ MC steps, discarding the initial 30 MC steps for more robust estimates. Hence $r = 1$ means an exact fit and so the closer r is to the unity, the better the fit. Here a and b are the linear coefficient and the slope in the linear fit $\ln\langle M\rangle$ versus $\ln t$, respectively. From b one estimates the exponent $\beta\nu/z$.

After one finishes this part of our refinement method (i), we proceed to the second part of refinement, the fine-scale stage (ii). Starting from the critical temperature $k_BT_c^{(1)}(q)/J_1$ obtained in the first stage, we use the process considering a more refined displacement, i.e., $\Delta^{(1)}(J_1/k_BT_c) = 1\times10^{-4}$. Thus, by using $J_1/k_BT_c^{(\min,1)} = J_1/k_BT_c^{(1)} - \Delta^{(0)}(J_1/k_BT_c)$ and $J_1/k_BT_c^{(\max,1)} = J_1/k_BT_c^{(1)} + \Delta^{(0)}(J_1/k_BT_c)$, we consider a new parametrization $J_1/k_BT_c = J_1/k_BT_c^{(\min,1)} + \Delta^{(1)}(J_1/k_BT_c)j$, with $j = 0,\ldots,41$. Hence we determine a new best temperature $k_BT_c^{(2)}/J_1$ corresponding to the maximum value of r.

Figure 2 shows the determination coefficient r as a function of temperature for two extremal cases $\alpha = 0.03$ and 0.27. The top plots correspond to the coarse-grained regime [the first refinement (i)] of the process $\Delta(J_1/k_BT) = 2\times10^{-3}$, while the bottom plots correspond to the fine-scale regime [the second refinement (ii)] $\Delta(J_1/k_BT) = 1\times10^{-4}$. The

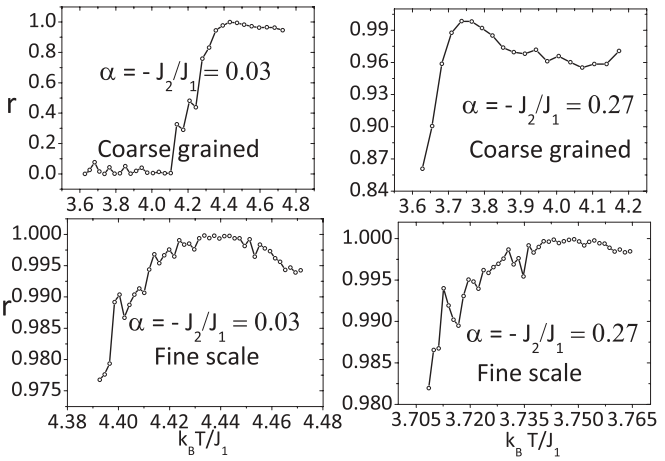

FIG. 2. Determination coefficient r as function of temperature for two cases $\alpha = 0.03$ and 0.27. The top plots correspond to coarse-grained regime (i) of the process $\Delta(J_1/k_BT) = 2\times10^{-3}$, while the bottom plots correspond to fine-scale regime (ii) of the process $\Delta(J_1/k_BT) = 1\times10^{-4}$.

estimated temperatures after two refinement states for all studied α values can be seen in Table I.

Since our final refinement has a precision of $\Delta(J_1/k_BT_c) = \Delta(\beta_c) = 10^{-4}$, which means $\Delta(T_c) = \Delta(\beta_c)T_c^2/[1+\Delta(\beta_c)T_c]$, we have a precision with three digits for temperature. Therefore, we show our results for critical temperatures with three significant elements (second column in Table I). It is important to mention that our estimates corroborate results from the literature: For example, for $\alpha = 0$ we have as the 3D Ising estimate $k_BT_c/J_1 = 4.513$, which yields excellent agreement with estimates via equilibrium Monte Carlo simulations [51]. For $\alpha = 0.27$ we have $k_BT_c/J_1 = 3.748$ as the best estimate for the LP's critical temperature, which also agrees with the estimate obtained by Henkel and Pleimling [18]: $k_BT/J_1 = 3.7475 \pm 0.0050$.

Here it is important to mention that in order to check the robustness of our method, we performed the same refinement process inverting the input, i.e., we set $k_BT/J_1 = 3.7475$ and we refine the value α. For the sake of simplicity, here we

TABLE I. Critical values obtained by refinement procedure after two stages (coarse grained and fine scale). Here the values obtained for $\alpha = 0$ and 0.27 correspond to our estimates of the critical temperatures of the 3D Ising model and the Lifshitz point, respectively.

$\alpha = -J_2/J_1$	k_BT_c/J_1	r
0.00	4.513	0.99993
0.03	4.434	0.99982
0.06	4.364	0.99990
0.09	4.289	0.99990
0.12	4.213	0.99993
0.15	4.126	0.99991
0.18	4.039	0.99988
0.21	3.956	0.99991
0.24	3.852	0.99989
0.27	3.748	0.99992

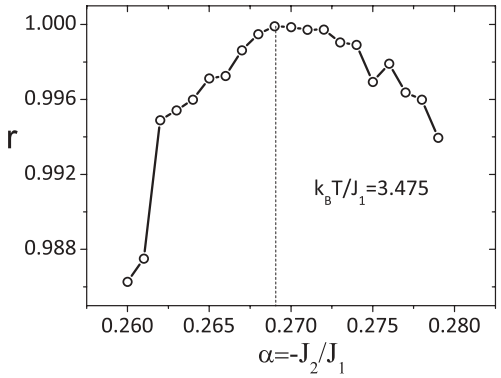

FIG. 3. Inverted refinement process: determination coefficient r as a function of α, which changes from 0.26 up to 0.28 by setting $k_B T/J_1 = 3.475$. Only one refinement process with $\Delta\alpha = 0.001$ was used. We obtain as the best estimate $\alpha = 0.269$, which shows that the method works in both ways.

perform only one refinement in a shorter interval spanning α values from 0.26 to 0.28 with $\Delta\alpha = 0.001$, which can be seen in Fig. 3. We find $\alpha = 0.269$ as the best estimate, which corroborates the expected value for $k_B T/J_1 = 3.7475$: $\alpha = 0.270(4)$.

Thus, once we have shown that our time-dependent simulations are calibrated and they corroborate the critical parameters of the main estimates of the literature, in the following section our focus is to calculate the critical exponents via time-dependent Monte Carlo simulations of the LP. First we present some exponents (z and β/ν) to monitor their behavior along the second-order transition. Then we show a detailed study for the Lifshitz point by calculating all (static and dynamic) critical exponents obtaining error bars by performing repetitions of simulations under different seeds. We also study some differences between rectangular and cubic lattices.

III. RESULTS

In this work we perform short-time Monte Carlo simulations in simple rectangular lattices of size $L_x \times L_y \times L_z$ and not only for $L_x = L_y = L_z = L$. Thus, at each instant t of the simulation, the value of any measured quantity is given by its average over n_s runs according to Eq. (14), which denotes an average over different repetitions (trajectories with different sequences of pseudorandom numbers).

In order to obtain error bars in our simulations for the LP, we use $n_b = 5$ sets of $n_s$runs corresponding to different seeds for the random numbers generator. For our calculations we first use cubic lattices $80 \times 80 \times 80$ to evaluate only two exponents z and β/ν along the second-order line by performing MC simulations using as input the critical parameters obtained in the preceding section. We monitor the behavior of these two exponents directly obtained as a function of $k_B T_c/J_1$.

For the Lifshitz point we use three different lattices $80 \times 80 \times 80$, $80 \times 80 \times 10$, and $120 \times 120 \times 10$ to study the possible distortions under rectangular regions. For each lattice size, the number of runs used in the simulations to obtain the exponents given in Eqs. (4), (6), (8), (5), (3), and (11) are shown in Table II.

TABLE II. Number of runs used in simulations for different size lattices.

No. of runs	$80 \times 80 \times 80$	$80 \times 80 \times 10$	$120 \times 120 \times 10$
$\beta/\nu z$ [Eq. (4)]	400	3200	1400
$(d - \frac{2\beta}{\nu})/z$ [Eq. (6)]	4000	3.2×10^4	1.4×10^4
$1/\nu z$ [Eq. (8)]	2000	1.6×10^4	7000
θ [Eq. (3)]	14000	14000	14000
θ [Eq. (5)]	28000	28000	28000
θ_g [Eq. (11)]	14000	14000	14000

Due to the axial anisotropy present in the ANNNI model, the critical behavior in the neighborhood of the LP is governed by two correlation lengths ξ_z and ξ_{xy} with different critical exponents ($\nu_z = \frac{1}{2}\nu_{xy}$) [14]. Therefore, at the LP, in the case of the simple cubic lattice, the resulting critical exponent ν may be either the exponent $\nu_z(\nu_{xy})$ or a combination of these exponents. Therefore, in order to calculate the static critical

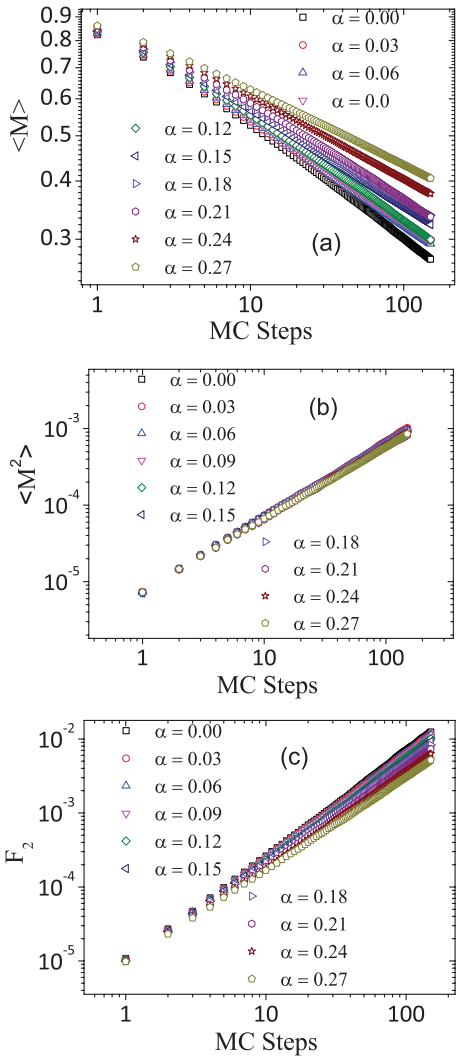

FIG. 4. (Color online) Time evolution of (a) $\langle M(t)\rangle_{m_0=1}$, (b) $\langle M^2(t)\rangle_{m_0=0}$, and (c) $F_2(t)$ for all critical temperatures previously estimated (corresponding to the different α values).

TABLE III. Monitoring of critical exponent z and the ratio of exponents β/ν along the second-order line previously estimated by time-dependent MC simulations.

$\alpha = -J_2/J_1$	z	β/ν
0.00	2.068	0.5118
0.03	2.069	0.4465
0.06	2.061	0.4807
0.09	2.076	0.4777
0.12	2.086	0.4746
0.15	2.137	0.4478
0.18	2.172	0.4334
0.21	2.197	0.4676
0.24	2.290	0.4082
0.27	2.338	0.3867

exponent ν for the Lifshitz point, we also consider not only cubic lattices in our study, but also rectangular lattices.

A. Monitoring the critical exponents of the ANNNI model

Using as input the critical parameters previously estimated in Sec. II, we have calculated the exponent z from the time dependence of the ratio F_2 [Eq. (7)] for cubic lattices with $L = 80$. Since z was calculated, the time evolution from the ordered state [Eq. (4)] that was used to compose F_2 is taken also to obtain an estimate of $\beta/\nu z$ and since we have an estimate of z by Eq. (10) we obtain an estimate of β/ν.

Performing MC simulations up to 150 MC steps and discarding the initial 30 MC steps for more robust estimates, we estimate these exponents for all α values corresponding to the critical temperatures that were previously obtained in Sec. II, considering the limits: 3D Ising like ($\alpha = 0$) up to the Lifshitz point ($\alpha = 0.27$). We set our simulations exactly at the temperatures obtained by our refinement procedure. The time evolution of the magnetization $\langle M(t)\rangle_{m_0=1}$, of its second moment $\langle M^2(t)\rangle_{m_0=0}$, and of $F_2(t)$ can be seen in Fig. 4.

The estimates of z and β/ν are summarized in Table III. We can observe that z is universal when J_2 is small, i.e., the interaction among second neighbors in the z direction is not pronounced and $z \approx 2.06$, which is expected for the universality class of the 3D Ising model.

However, in the neighborhood of the Lifshitz point, the exponent z has a sensitive increase in relation to the Ising-like behavior. The ratio of exponents β/ν changes in an interval [0.38,0.52], but not monotonically, as occurs with z. In the following section we study all the details of the Lifshitz point, taking into consideration error bars obtained by considering simulations with different seeds since we observed a notorious difference between this point ($\alpha = 0.27$) and the authentic 3D Ising model ($\alpha = 0.0$).

B. Lifshitz point

In this section we finally present a detailed study of critical exponents of the Lifshitz point. Initially we considered cubic lattices $L_x = L_y = L_z = 80$. Here it is important to stress

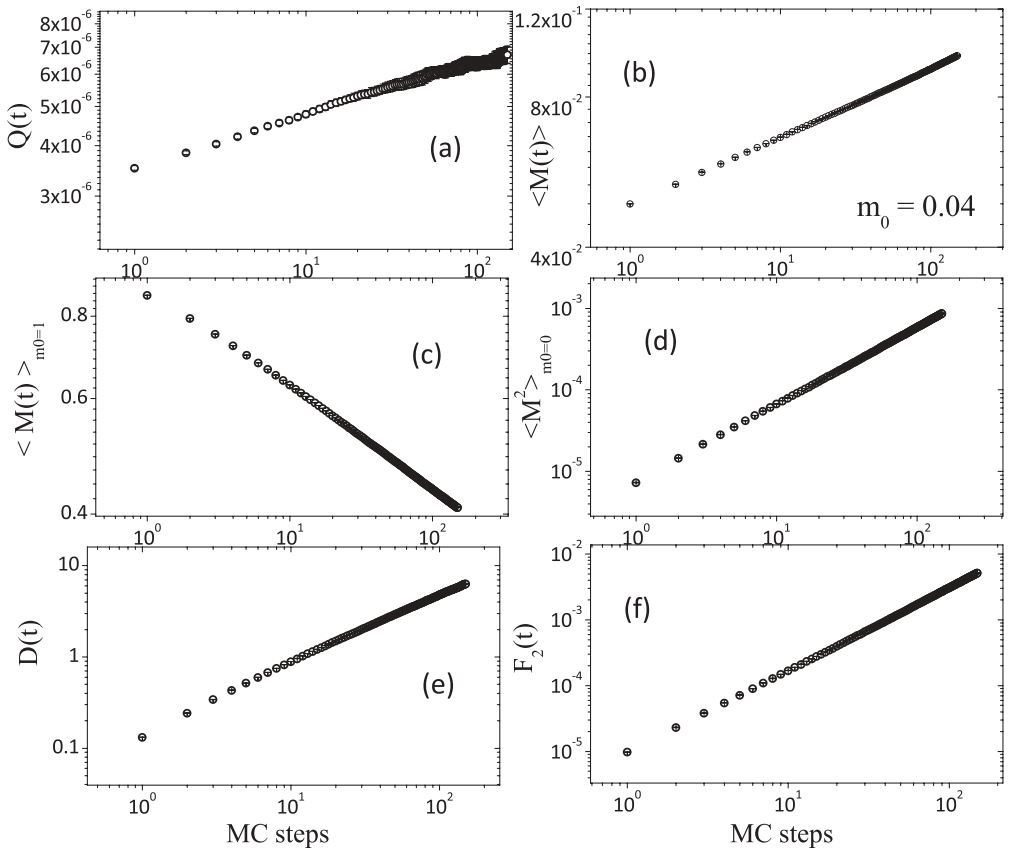

FIG. 5. (a) A log-log plot of $Q(t)$ against t for the lattice size $80 \times 80 \times 80$ for the Lifshitz point using $\alpha = 0.27$ and $k_B T_c/J_1 = 3.7475$. (b)–(f) correspond to the same plot for (b) $\langle M(t)\rangle_{m_0=0.04}$, (c) $\langle M(t)\rangle_{m_0=1}$, (d) $\langle M^2(t)\rangle_{m_0=0}$, (e) $D(t)$, and (f) $F_2(t)$.

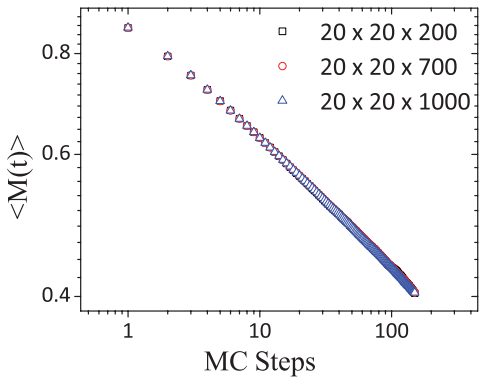

FIG. 6. (Color online) A log-log plot of $\langle M(t)\rangle$ against t obtained from the simulations performed for the lattice size $20 \times 20 \times L_z$, where $L_z > 20$ and $m_0 = 1$(ordered initial state).

that we used $\alpha = 0.27$ and $k_B T_c/J_1 = 3.7475$ (the estimate obtained by Henkel and Pleimling [18]) to perform the simulations.

From Monte Carlo simulations we obtained the exponents for the Lifshitz point defined by Eqs. (7) [which uses Eqs. (4) and (6)], (8), (3), and (5). The log-log curves for the Lifshitz point for these quantities considering the error bars obtained by five different seeds are shown in Fig. 5. For Eq. (3) we show (for the sake of simplicity) only the evolution for $m_0 = 0.04$.

We have obtained the critical exponents $\beta = 0.226(2)$, $\nu = 0.60(1)$, $z = 2.34(2)$, $\theta = 0.17(2)$ [from Eq. (5)], and $\theta = 0.163(3)$ [Eq. (3)]. For this last case the results were obtained by performing simulations with three different initial magnetizations $m_0 = 0.02$, 0.04, and 0.08. By obtaining the exponent for each value with error bars obtained by five seeds, we considered a linear fit to obtain an extrapolation $m_0 \to 0$, which corresponds to the linear coefficient in the fit θ versus m_0.

To verify whether the ferromagnetic ordering is affected by increasing the linear dimension L_z, we perform extra MC simulations for the temporal evolution of magnetization from the ordered initial state $m_0 = 1$, considering the following rectangular lattices: $20 \times 20 \times 200$, $20 \times 20 \times 700$, and $20 \times 20 \times 1000$. Here we are only interested in the qualitative

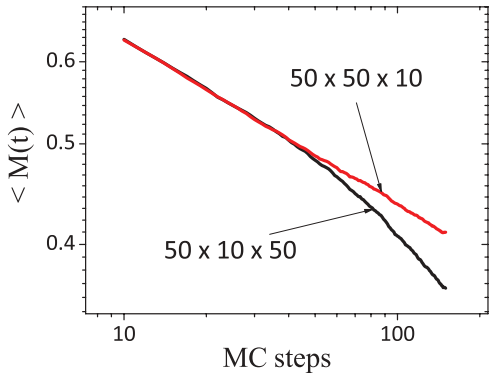

FIG. 7. (Color online) A log-log plot of $\langle M(t)\rangle$ against t obtained from the simulations performed for the lattice sizes $50 \times 50 \times 10$ and $50 \times 10 \times 50$, starting from the initial condition $m_0 = 1$(ordered initial state). The order parameter decays faster for the lattice with smaller xy planes.

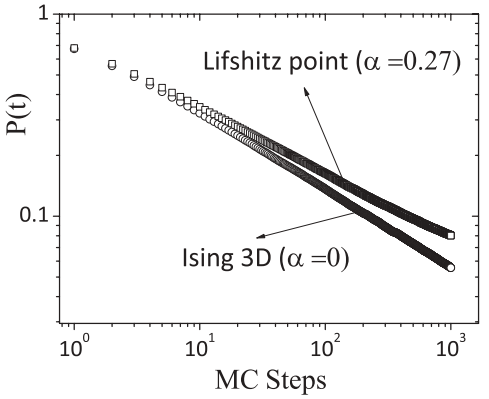

FIG. 8. Time evolution of global persistence for $\alpha = 0$ (3D Ising model) (with $k_B T/J_1 = 4.513$) and $\alpha = 0.27$ (Lifshitz point) (with $k_B T/J_1 = 3.7475$).

plots of $\langle M(t)\rangle$ versus t. We used in all cases just $n_s =$ 400runs. In Fig. 6 we find identical log-log plots for the different rectangular lattices analyzed, which corroborates that ferromagnetic ordering does not depend on linear dimension L_z, despite the increase of the total number of spins on the lattice.

Since the order parameter is the magnetization and the xy interactions are ferromagnetic, the ordering occurs mainly due to these interactions. In contrast, there are competing interactions along the z axis, which cannot sustain the ferromagnetic ordering of the system. This fact is illustrated in Fig. 7, where the magnetizations $\langle M(t)\rangle$ obtained from simulations for lattices $50 \times 50 \times 10$ and $50 \times 10 \times 50$ are shown. In Fig. 7 we clearly see that the order parameter decays faster for the lattice with a smaller xy plane ($50 \times 10 \times 50$).

Therefore, we conclude that the best results will be obtained from lattices with bigger xy planes, irrespective of the value L_z. However, we must stress here that these conclusions are valid in the short-time regime. In contrast, via equilibrium MC simulations, which were performed in a simple cubic lattice ($24 \times 24 \times 24$), Kaski and Selke [17] obtained the critical exponent $\nu = 0.51(4)$ corresponding to a combination of the exponents ν_z and ν_{xy} due to anisotropy present in the LP. In order to obtain the critical exponent $\nu_z = 0.33(3)$ shown in Table IV, which shows exponents for our comparison extracted from the literature obtained for different methods, these authors divided the lattice into subcells $24 \times 24 \times L$. By

TABLE IV. Static critical exponents β, ν_z, and $\nu_{xy} = 2\nu_z$ at the LP extracted from the literature.

Exponent	First-order ε[a]	Second-order ε[b]	Monte Carlo	MnP[c]
β	1/4	0.220	0.19(2)[d] 0.238(5)[e]	
ν_z	5/16	0.348	0.33(3)	0.30(2)
ν_{xy}	5/8	0.696	0.66[d]	0.60(4)

[a]Reference [14].
[b]Reference [54].
[c]Reference [55].
[d]Reference [17].
[e]Reference [18].

TABLE V. Static and dynamic critical exponents β, z, ν_{xy}, θ, and θ_g obtained in the present work for different lattice sizes.

Exponent	$80 \times 80 \times 80$	$80 \times 80 \times 10$	$120 \times 120 \times 10$
β	0.226(2)	0.227(1)	0.229(2)
z	2.34(2)	2.296(2)	2.30(1)
ν_{xy}	0.60(1)	0.615(3)	0.618(4)
θ	0.17(2) [Eq. (5)]	0.16(2) [Eq. (5)]	0.16(2) [Eq. (5)]
	0.163(3) [Eq. (3)]	0.180(6) [Eq. (3)]	0.184(1) [Eq. (3)]
θ_g	0.336(4)	0.330(5)	0.336(6)

using this procedure, Kaski and Selke [17] were able to capture the spacial correlations ξ_z and from the slope of Binder's cumulant [52,53] they estimated the value of ν_z, which is also shown in Table IV.

In the following we show the results obtained in this work for the lattice sizes $80 \times 80 \times 10$ and $120 \times 120 \times 10$. We estimated the critical exponents $\beta = 0.227(1)$, $z = 2.296(3)$, and $\nu = 0.615(3)$ for the $80 \times 80 \times 10$ lattice and $\beta = 0.229(2)$, $z = 2.30(1)$, and $\nu = 0.618(4)$ for the $120 \times 120 \times 10$ lattice.

Finally, we also study the global persistence for the Lifshitz point. For a simple comparison, we also performed simulations for $\alpha = 0$ (which corresponds to the three-dimensional Ising model). The same procedure used in the previous simulations (five seeds to obtain error bars) was replicated here as well. Figure 8 shows the different time evolutions of global persistence $P(t)$ for the two different points.

For lattices $80 \times 80 \times 80$ we obtain $\theta_g = 0.336(4)$ for the Lifshitz point. This value is smaller than the $\theta_g = 0.384(6)$ found for the 3D Ising model. This value for the Lifshitz point seems to be corroborated for rectangular lattices (compatible with error bars) where we observed only small changes for rectangular lattices $80 \times 80 \times 10$ and $120 \times 120 \times 10$ (see the last row in Table V).

Table V summarizes the results of the static and dynamic critical exponents obtained in this work. These results are in very good agreement with the critical exponents obtained in previous works, shown in Table IV.

IV. SUMMARY AND DISCUSSION

In this work we estimated the dynamic critical exponents θ, θ_g, and z at the Lifshitz point of the ANNNI model by means of time-dependent Monte Carlo simulations. We have also obtained the static and critical exponents β and ν by exploiting scaling relations, valid in the short-time regime (out of equilibrium), involving the order parameter and its second moment. Our estimates (see Table V) are in very good agreement with previous experimental and theoretical works (see Table IV).

Moreover, we applied a refinement procedure to estimate several parameters for the critical points along the second-order transition line from the 3D Ising point $-J_2/J_1 = 0$ up to the Lifshitz point $-J_2/J_1 = 0.27$ and followed the behavior of some exponents along this line. We observed that z is universal when J_2 is small, i.e., the interaction among second neighbors in the z direction is not pronounced, resulting in $z \approx 2.06$, which is expected for the universality class of the 3D Ising. However, in the neighborhood of the Lifshitz point, the exponent z has a sensitive increase resulting in $z \approx 2.34$. Finally, we also observe power-law behavior for the global persistence $P(t)$ (the probability that the sign of the magnetization does not change until the time t starting from random configurations with small magnetization). We find $\theta_g = 0.336(4)$ ($\alpha = 0.27$) for the LP, which is smaller than the 3D Ising estimate ($\alpha = 0$) of $\theta_g = 0.384(6)$, see for example [45].

ACKNOWLEDGMENTS

The authors were partly supported by the Brazilian Research Council CNPq. We thank CESUP (Super Computer Center of Federal University of Rio Grande do Sul) as well as Professor Leonardo G. Brunet (IF-UFRGS) for the available computational resources. We are grateful for support from Clustered Computing (ada.if.ufrgs.br) and to Professor Mendeli H. Vainstein (IF-UFRGS) for carefully reading our manuscript.

[1] P. Bak, Rep. Prog. Phys. **45**, 587 (1982).
[2] G. Toulouse, Commun. Phys. **2**, 115 (1977).
[3] B. R. Cooper, Solid State Phys. **21**, 393 (1968).
[4] M. A. Ruderman and C. Kittel, Phys. Rev. **96**, 99 (1954).
[5] T. Kasuya, Prog. Theor. Phys. **16**, 45 (1956).
[6] K. Yosida, Phys. Rev. **106**, 893 (1957).
[7] R. J. Elliott, Phys. Rev. **124**, 346 (1961).
[8] M. E. Fisher and W. Selke, Phys. Rev. Lett. **44**, 1502 (1980).
[9] W. Selke, Phys. Rep. **170**, 213 (1988).
[10] J. M. Yeomans, in *Solid State Physics*, edited by H. Ehrenreich and D. Turnbull (Academic, San Diego, 1988), Vol. 41, pp. 151–200.
[11] W. Selke, in *Phase Transitions and Critical Phenomena*, edited by C. Domb and J. L. Lebowitz (Academic, London, 1992), Vol. 15, pp. 1–72.
[12] P. Bak and J. von Boehm, Phys. Rev. B **21**, 5297 (1980).
[13] T. Garel and P. Pfeuty, J. Phys. C **9**, L245 (1976).
[14] R. M. Hornreich, M. Luban, and S. Shtrikman, Phys. Rev. Lett. **35**, 1678 (1975).
[15] S. Redner and H. E. Stanley, Phys. Rev. B **16**, 4901 (1977).
[16] W. Selke, Z. Phys. B **29**, 133 (1978).
[17] K. Kaski and W. Selke, Phys. Rev. B **31**, 3128 (1985).
[18] M. Henkel and M. Pleimling, Comput. Phys. Commun. **147**, 419 (2002).
[19] U. Wolff, Phys. Rev. Lett. **62**, 361 (1989).
[20] R. M. Hornreich, J. Magn. Mater. **15**, 387 (1980).
[21] Z. Mo and M. Ferer, Phys. Rev. B **43**, 10890 (1991).
[22] C. C. Becerra, Y. Shapira, N. F. Oliveira Jr., and T. S. Chang, Phys. Rev. Lett. **44**, 1692 (1980).
[23] Y. Shapira, C. C. Becerra, N. F. Oliveira Jr., and T. S. Chang, Phys. Rev. B **24**, 2780 (1981).

[24] V. Bindilatti, C. C. Becerra, and N. F. Oliveira Jr., Phys. Rev. B **40**, 9412 (1989).
[25] Z. B. Li, L. Schülke, and B. Zheng, Phys. Rev. E **53**, 2940 (1996).
[26] R. Folk and W. Selke, Phys. Lett. A **69**, 255 (1978).
[27] A. Basu and J. K. Bhattacharjee, J. Phys. A **37**, 1111 (2004).
[28] T. Ala-Nissila, J. D. Gunton, and K. Kaski, Phys. Rev. B **37**, 179 (1988).
[29] M. Cheon and I. Chang, Phys. Rev. Lett. **86**, 4576 (2001).
[30] H. K. Janssen, B. Schaub, and B. Shmittmann, Z. Phys. B **73**, 539 (1989).
[31] D. A. Huse, Phys. Rev. B **40**, 304 (1989).
[32] B. Zheng, Int. J. Mod. Phys. B **12**, 1419 (1998).
[33] E. V. Albano, M. A. Bab, G. Baglietto, R. A. Borzi, T. S. Grigera, E. S. Loscar, D. E. Rodriguez, M. L. Rubio Puzzo, and G. P. Saracco, Rep. Prog. Phys. **74**, 026501 (2011).
[34] T. Tome and M. J. de Oliveira, Phys. Rev. E **58**, 4242 (1998).
[35] E. Arashiro and J. R. Drugowich de Felício, Phys. Rev. E **67**, 046123 (2003).
[36] R. da Silva, N. A. Alves, and J. R. Drugowich de Felício, Phys. Lett. A **298**, 325 (2002).
[37] R. da Silva and J. R. Drugowich de Felício, Phys. Lett. A **333**, 277 (2004); H. A. Fernandes, E. Arashiro, J. R. Drugowich de Felício, and A. A. Caparica, Physica A **366**, 255 (2006); E. Arashiro, H. A. Fernandes, and J. R. Drugowich de Felício, *ibid.* **388**, 4379 (2009).
[38] C. S. Simões and J. R. Drugowich de Felício, Mod. Phys. Lett. B **15**, 487 (2001).
[39] N. Alves Jr. and J. R. Drugowich de Felício, Mod. Phys. Lett. B **17**, 209 (2003).
[40] T. Tomé and J. R. Drugowich de Felício, Mod. Phys. Lett. B **12**, 873 (1998).
[41] R. da Silva, N. A. Alves, and J. R. Drugowich de Felício, Phys. Rev. E **66**, 026130 (2002).
[42] H. A. Fernandes, R. da Silva, and J. R. Drugowich de Felício, J. Stat. Mech. (2006) P10002.
[43] E. Arashiro, J. R. Drugowich de Felício, and U. H. E. Hansmann, Phys. Rev. E **73**, 40902 (2006); J. Chem. Phys. **126**, 045107 (2007).
[44] R. da Silva, J. R. Drugowich de Felício, and A. S. Martinez, Phys. Rev. E **85**, 066707 (2012).
[45] S. N. Majumdar, A. J. Bray, S. J. Cornell, and C. Sire, Phys. Rev. Lett. **77**, 3704 (1996).
[46] S. N. Majumdar and C. Sire, Phys. Rev. Lett. **77**, 1420 (1996).
[47] H. K. Janssen, in *From Phase Transitions to Chaos*, edited by G. Györgyi, I. Kondor, L. Sasvári, and T. Tél, *Topics in Modern Statistical Physics* (World Scientific, Singapore, 1992).
[48] R. da Silva, N. A. Alves, and J. R. Drugowich de Felício, Phys. Rev. E **67**, 057102 (2003).
[49] R. da Silva, A. L. C. Bazzan, A. T. Baraviera, and S. R. Dahmen, Physica A **371**, 610 (2006).
[50] R. da Silva, M. Zembrzuski, F. C. Correa, and L. C. Lamb, Physica A **389**, 5460 (2010).
[51] W. Janke and R. Villanova, Nucl. Phys. B **489**, 679 (1997).
[52] K. Binder, Phys. Rev. Lett. **47**, 693 (1981).
[53] K. Binder, Z. Phys. B **43**, 119 (1981).
[54] M. Shpot and H. W. Diehl, Nucl. Phys. B **612**, 340 (2001).
[55] Y. Shapira, *Multicritical Phenomena*, edited by R. Pynn and A. Skjeltorp, Vol. 106, NATO ASI Series, pp. 35–52 (1984).